Proceedings of the 14th International Heat Transfer Conference
IHTC-14
August 8-13, 2010, Washington D.C., USA

IHTC14-23182

THERMAL AND ELECTROCHEMICAL CELL DESIGN AND ITS EXPERIMENTAL ASSESSMENT FOR MICRO SOFC SYSTEM

Satoshi Usui
Department of Mechanical Engineering,
The University of Tokyo,
Hongo, Tokyo, Japan

Mina Nishi
Department of Mechanical Engineering,
The University of Tokyo,
Hongo, Tokyo, Japan

Naoki Shikazono
Department of Mechanical Engineering,
The University of Tokyo,
Hongo, Tokyo, Japan

Nobuhide Kasagi
Department of Mechanical Engineering,
The University of Tokyo,
Hongo, Tokyo, Japan

ABSTRACT

A numerical simulation tool to predict the performance of a tubular SOFC is developed. For the convenience of the infrastructure, it has become more important to consider feeding hydrocarbon fuels like methane, which would be widely used, rather than hydrogen. Although it is well known that the performance of an SOFC drops largely when methane is fed compared with hydrogen, the reason for this is not yet well explained and thus prevents efficiently constructing an optimized SOFC system. Therefore, the present investigation is carried out to clarify how an SOFC performs when different fuels are fed. The calculation based on one-dimensional computation is carried out by introducing the parameters of actual electrode microstructures, obtained from the images taken by the focused ion beam scanning electron microscope (FIB-SEM). Values are adapted in calculating the ohmic, activation and concentration overpotentials. Proper experiments were also carried out to verify the validity of the numerical simulation. Although slight errors are found in the calculation results for fuels with high steam concentration, performances of hydrogen and methane fed cells were well predicted. Temperature distribution within the cell is also clearly shown. Through the present investigation, the performance drop, when the fuel is changed from hydrogen to methane, is found mainly caused by the temperature distribution of the cell that gives a concrete guide to construct an SOFC system.

1. INTRODUCTION

There has been a rapid growth of interest towards solid oxide fuel cell (SOFC) because of its high efficiency and fuel flexibility. Although field tests for some kW order SOFC systems are currently underway, there are still many issues to be resolved, e.g. cost and durability of the cell. It is also noted that small SOFC systems of a few Watt capacity is also of great interest since they are superior in its compactness and applicability for mobile usage.

Designing such SOFC systems is a multi-physics and multi-scale problem, since heat and mass transfer with electrochemical reaction should be considered from the macroscopic system-scale down to the microscopic scale in SOFC micro porous electrodes. In the present study, the cell-level computational model for heat and mass transfer including electrochemical reaction in SOFC, which was first reported by Suzuki et al. [1] and later modified by Sekiguchi et al. [2], is extended to methane fuel. Suzuki et al. [1] used the model for a flat-tube SOFC with externally reformed methane, and calculated the thermo-fluidic characteristics of the cell including chemical reaction. Sekiguchi et al. [2] adjusted the model for a tubular SOFC, improved the numerical prediction, and obtained good agreement with their own experimental results by introducing dusty gas model (DGM) to the gas diffusion term. Presently, an additional model is adopted to take account of an endothermic internal reforming process of methane in a micro anode-supported tubular SOFC. Moreover, important physical parameters such as a three-phase boundary (TPB) density and tortuosity factor are directly measured from the cross-sectional images of the anode acquired by FIB-SEM and used in the numerical prediction of SOFC characteristics.

To assess the validity of the present model, experiments are carried out with a tubular SOFC in a high temperature furnace

under various conditions. The fuel compositions of hydrogen, steam and methane are changed systematically for comparisons with the predicted cell performance. The knowledge obtained here will be fed back to the designing of an SOFC system.

NOMENCLATURE

A	surface area [m^2]
d	pore diameter [m]
D	diffusion coefficient [m^2/s]
E	electromotive force [V]
F	Faraday constant
G	Gibbs free energy [J/mol]
Gr	Grashof number
h	heat transfer coefficient [W/m^2K]
i	current density [A/cm^2]
M	molar mass [g/mol]
N	mole flux [mol/m^2s]
p	partial pressure [Pa]
P	total pressure [Pa]
Nu	Nusselt number
Pr	Prandtl number
Q	heat flux [W]
Ra	Rayleigh number
T	temperature [K]
y	mole fraction

Greek Symbols

ε	emissivity or porosity
ϕ	electric potential [V]
γ	pre-exponential factor [A/cm^2]
η	overpotential [V]
λ	thermal conductivity [W/mK]
ρ	density [g/cm^2]
σ	conductivity [S/m]
τ	tortuosity factor
ν	kinematic viscosity [m^2/s]

Subscripts

act	activation
an	anode
ca	cathode
el	electron
io	ion
k	Knudsen
reac	reaction

2. EXPERIMENTAL TEST RIG AND CONDITIONS

The experimental setup is schematically shown in Fig. 1. The test rig consists of a high temperature furnace, a pre-heated fuel supplier, an air pre-heater and an electrical measurement unit. Computer with pre-programmed software operates the furnace and mass flow controllers so that all the experiments

Table 1. Experimental fuel condition

	#1	#2	#3	#4	#5	#6	#7	#8
H_2 [sccm]	20	20	20	20	0	0	0	0
H_2O [sccm	0	3	6	9	5	6	9	12
CH_4 [sccm]	0	0	0	0	5	5	5	5
Steam ratio [%]	0	13	23	31	-	-	-	-
S/C [-]	-	-	-	-	1.0	1.2	1.8	2.4

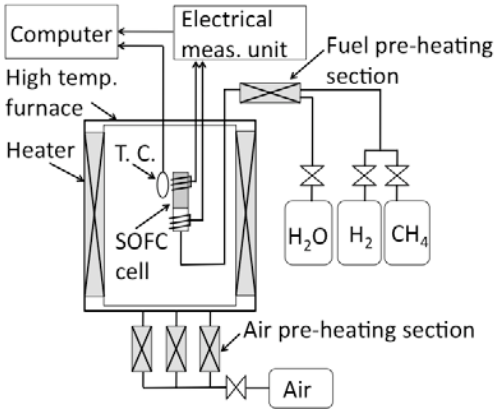

Fig. 1. Schematic presentation of experimental test rig

are carried out in well-controlled manner. A tubular anode-supported SOFC is prepared by the following procedure[3]. First, electrolyte Zirconium powder (Tohso, TZ-3Y-E) is dip-coated on the extruded tubular anode, and is co-sintered at T = 1400 ℃ for 3 hours. LSM and YSZ cermet (50% to 50% content) is then dip coated and sintered on the electrolyte layer, and finally LSM on the cermet layer. Both layers are sintered at T = 1100 ℃ for 3 hours. For electrical probe, ϕ = 0.4 mm Pt wire is sintered on the electrodes by Ag-paste (Dotite) at T = 800 ℃. Before carrying out the verification experiments, the SOFC is reduced by hydrogen in the furnace at T = 750 ℃ for over 40 hours. During initial electrical loading, an increase in the concentration overpotential and a decrease in the activation overpotential were observed. Therefore, the cell was loaded with 0.1 A/cm^2 for over 30 hours after reduction, and the impedance was measured every 2 hours to make sure that the SOFC' s performance had reached to a steady state.

The experimental fuel condition is summarized in Table 1. The furnace temperature is kept constant at T = 750 ℃ for all experiments. The temperature is measured by a thermo couple (T.C.) on the surface of the cathode of SOFC. In the first set of experiments, hydrogen is applied as a fuel and steam is varied from 13% to 31%. In the second set of experiments, methane and steam mixed fuel is applied. The volume flow

rate of methane is kept constant as 5 sccm, and the steam volume flow rate is varied from 5 to 12 sccm to test various steam-carbon ratios (S/C = 1.0 to 2.4).

3. OBTAINING MICROSTRUCTURAL PARAMETERS BY FIB-SEM

In order to obtain the 3D microstructural parameters of the SOFC anode, FIB-SEM equipped with a Gemini FE-SEM column (NVision 40,Carl Zeiss), a zeta FIB column (SIINT), and a multichannel gas injection system (SIINT), is used. The sample is pre-treated before measurement by infiltrating epoxy resin under vacuum in order to distinguish the pores from Ni and YSZ phases. The observation area is coated with carbon to prevent the sample from charging due to ion-beam exposure. Totally, 214 slices of cross-sectional images (27.91 nm per pixel) at 58.25 nm pitch are re-constructed by the method of Iwai et al. [4] to produce a volume of 21.21 × 14.51 × 12.41 μm^3. Ni, YSZ, and pore phases are distinguished by their brightness values after pretreatment with various noise filters. The reconstructed model is re-meshed to 100 nm cubic voxels.

SEM image and reconstructed 3D structure are shown in Figs. 2 and 3, respectively. Since the thickness of the obtained structure is not large enough to reproduce the actual anode thickness, mirrored images are repeated in *z* direction as shown in Fig. 4. It's tortuosity factor is calculated using the lattice Boltzmann method (LBM), and TPB density using the centroid method. Values obtained from this image are shown in Table 2.

4. NUMERICAL MODEL

A finite volume method is used to solve the flow in a tubular SOFC as shown in Fig. 5. It is modeled by a one-dimensional (1D) computational system. Heat and mass transfer in the axial direction is calculated, while gas diffusion and ion/electron conduction in the radial direction is simulated independently from axial flow effect. The cell is placed inside a heat chamber. A pre-heated and pre-mixed fuel enters the cell and combusts when it reaches the fuel outlet region of the cell where it mixes with the air supplied. A sufficient amount of air, with the composition of 20% oxygen and 80% nitrogen, is fed from the bottom of the chamber. The chamber wall is kept at 750℃, and the cell is heated mainly by radiation heat transfer from the wall surface.

The radiation heat transfer between the heater wall and the cell is governed by the following equation:

$$Q = \varepsilon_{cell} A_{cell} \sigma \left(T_{wall}^4 - T_{cell}^4 \right) \quad (1)$$

where σ is the Stephan-Boltzmann constant. The emissivity of the cell is given the gray approximation value for porous ceramic $\varepsilon_{cell} = 0.8$. The heat transfer between the cell surface and the surrounding air is determined by the following equation:

$$Q = hA(T_{wall} - T_{air}) \quad (2)$$

With natural convection assumed around the cell, the corresponding *Nu* is calculated. The local *Nu* of a cylinder at height *x* $(Nu_x)_c$ can be expressed by the following equation:

Table 2 Anode Structural Parameters

Properties		Value
3D-TPB density L_{TPB} [10^{12} m/m^3]		1.373
Tortuosity factor τ	Pore	2.950
	YSZ	4.287
	Ni	13.128
Volume fraction ε	Pore	0.319
	YSZ	0.378
	Ni	0.303

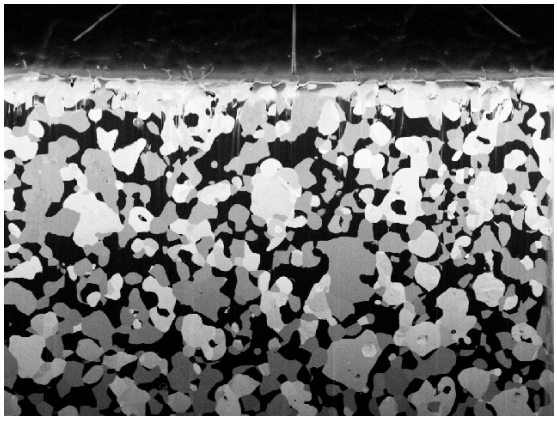

Fig. 2. SEM image of anode

Fig. 3. Reconstructed 3D image of anode

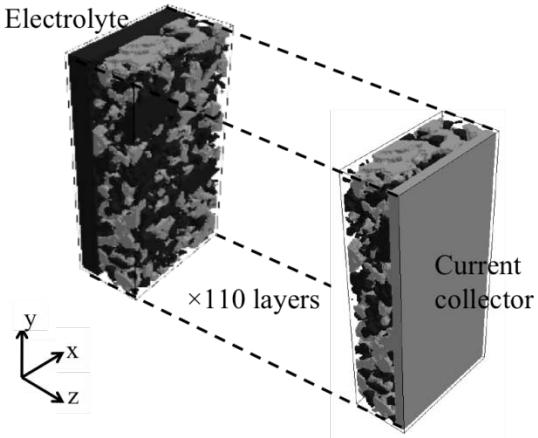

Fig. 4. Layered reconstructed structure

$$\frac{(Nu_x)_c}{(Nu_x)_p} = 1 + 0.43\left[\frac{x/r_o}{(Nu_x)_p}\right] \quad (3)$$

where r_o the radius of the cylinder, and $(Nu_x)_p$ is the Nusselt value for vertical plate, given by

$$(Nu_x)_p = C_l(\nu_\infty/\nu_w)^{0.21} Ra_x^{1/4} \quad (4)$$

Here, C_l is given as a function of the Prandtl number:

$$C_l = 3/4\left\{\Pr/(2.4 + 4.9\sqrt{Pr} + 5Pr)\right\}^{1/4} \quad (5)$$

When the fluid is air, $(\nu_\infty / \nu_w) = 1$ is assumed. The Rayleigh number *Ra* is given by

$$Ra = Pr \cdot Gr_x = Pr \cdot g\beta(T_w - T_\infty)x^3/\nu^2 \quad (6)$$

The Pr number is assumed constant, and given the value of 0.717.

For the calculation of electromotive force (E.M.F.) and overpotentials, the equivalence circuit shown in Fig. 6 is assumed. The E.M.F. for the oxidation of hydrogen can be calculated as:

$$E = \frac{G_{H_2} + 1/2G_{O_2} - G_{H_2O}}{2F} = \frac{-\Delta G^\circ_{H_2O}}{2F} + \frac{RT}{2F}\ln\left[\frac{p_{H_2}p_{O_2}}{p_{H_2O}}\right] \quad (7)$$

where G_{H2O} is derived by using the Gibbs-Helmholtz equation:

$$\left[\frac{\partial}{\partial T}\left(\frac{\Delta G^\circ_{H_2O}}{T}\right)\right]_p = \frac{-\Delta H^\circ_{H_2O}}{T^2} = \frac{-1}{T^2}\left(\Delta H^\circ_{H_2O}\Big|_{T=298.15K} + \int c_p dT\right) \quad (8)$$

In the calculation of each overpotential, microstructural parameters obtained using FIB-SEM are applied in order to give predictions of high accuracy. Tortuosity factor τ and volume ratio ε are used to predict the effective ionic and electronic conductivities by the following equation:

$$\sigma^{\text{eff}} = \frac{\varepsilon}{\tau}\sigma \quad (9)$$

Tortuosity factor τ and porosity ε values are also used in simulating the gas diffusion inside the porous anode. In this study, the dusty gas model (DGM) is used, which is reported to predict concentration overpotential of an SOFC anode with higher reliability compared with Fick's and Stefan-Maxwell's model[5]. If constant total pressure is assumed, dusty gas model can be represented by the following equation:

$$\frac{N_i}{D_{i,k}} + \sum_{j=1, j\neq i}^{n}\frac{y_jN_i - y_iN_j}{D_{i,j}} = -\frac{p}{RT}\frac{dy_i}{dr} \quad (10)$$

Here, the binary diffusion coefficient and Knudsen diffusion coefficient are represented by the following equations:

$$D_{ij} = 1.8829\times10^{-2}\left[\frac{\left\{T^3\left(M_i + M_j\right)/M_iM_j\right\}^{1/2}}{p\zeta_{ij}^2\Omega_D}\right] \quad (11)$$

$$D_k = \frac{2}{3}\left(\frac{8RT}{\pi M}\right)^{0.5}\frac{d_p}{2} \quad (12)$$

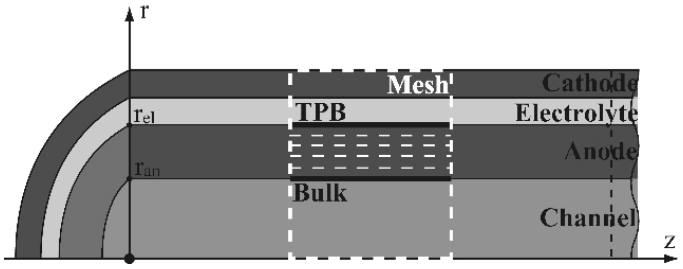

Fig. 5. Tubular SOFC model

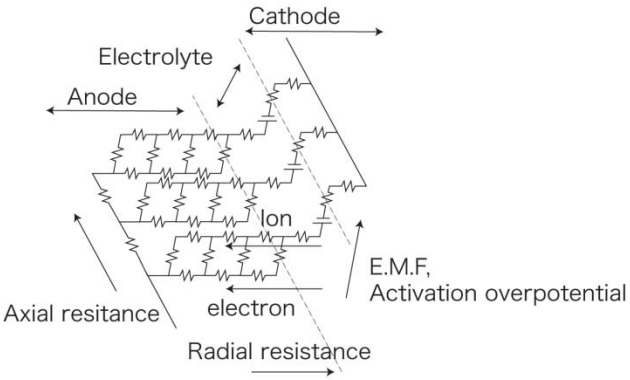

Fig. 6. Equivalence circuit of SOFC

The hydrogen flux N_{H2} at the electrolyte surfais assumed to be equal to the rate of consumption due to electrochemical reaction, and given the following equation

$$N_{H_2} = \frac{r_{el}}{r}\frac{i}{2F} \quad (13)$$

where r_{el} is the distance from the center to the electrolyte layer. By using the Graham's law

$$\sum_{i=1}^{n} N_i\sqrt{M_i} = 0 \quad (14)$$

and Eq. (13), Eq. (10) can be re-stated as follows:

$$\frac{d^2y_1}{dr^2} + \frac{\alpha}{D_{12}^{\text{eff}}}\left[\frac{1}{D_{1,k}^{\text{eff}}} + \frac{1}{D_{13}^{\text{eff}}} + (1-y_3)\left(\frac{1}{D_{12}^{\text{eff}}} - \frac{1}{D_{13}^{\text{eff}}}\right) - \frac{\alpha y_1}{D_{12}^{\text{eff}}}\right]^{-1} \times\left(\frac{dy_1}{dr}\right) - \frac{i}{2F}\frac{r_{el}}{r^2} = 0 \quad (15)$$

$$\alpha = 1 - \sqrt{\frac{M_1}{M_2}}, D^{\text{eff}} = \frac{\varepsilon}{\tau}D \quad 1$$

The diffusion calculation is conducted in the porous anode layer, which is split into two layers; transport diffusion layer, and effective reaction layer. In the transport diffusion layer, the gas mainly diffuses through the pore center towards the electrolyte. In the effective reaction layer, which is located between the transport diffusion layer and the electrolyte, hydrogen reacts at TPB. The diffusion path toward TPB is considered to be more inflected compared to the bulk diffusion path. Therefore, this phenomenon is modeled by applying

different mean pore diameters to each layer. The transport diffusion layer, given 80% of the total thickness, posses a mean pore diameter of 200 nm, whereas the effective reaction layer, being the remaining 20% of the porous media, was given a pore diameter of 14 nm.

The concentration overpotential can now be calculated by using the above equations. Boundary condition can be expressed as follows:

$$\left.\frac{\mathrm{d}y_1}{\mathrm{d}r}\right|_{r=r_{an}} = \frac{r_{el}}{r}\frac{iART}{2PF}\left[\frac{1}{D_{1,k}^{\mathrm{eff}}}+\frac{1}{D_{13}^{\mathrm{eff}}}+(1-y_3)\left(\frac{1}{D_{12}^{\mathrm{eff}}}-\frac{1}{D_{13}^{\mathrm{eff}}}\right)-\frac{\alpha y_1}{D_{12}^{\mathrm{eff}}}\right] \tag{16}$$

(17)

The activation overpotential is governed by the following Butler-Volmer like equation:

$$i_{\mathrm{reac}} = i_0 L_{\mathrm{TPB}}\left\{\exp(\frac{\alpha 2F}{RT}\eta_{\mathrm{act}})-\exp(-\frac{(1-\alpha)2F}{RT}\eta_{\mathrm{act}})\right\} \tag{18}$$

where i_o represents exchange current density, which can be expressed for anode[6] and cathode[7] as follows:

$$i_{0,\mathrm{an}} = \gamma\left(\frac{p_{\mathrm{H_2,TPB}}}{p_{\mathrm{bulk}}}\right)^{-0.03}\left(\frac{p_{\mathrm{H_2O,TPB}}}{p_{\mathrm{bulk}}}\right)^{0.4}\exp\left(-\frac{E_{\mathrm{act,an}}}{RT}\right) \tag{19}$$

$$i_{0,\mathrm{ca}} = \gamma\left(\frac{p_{\mathrm{O_2,TPB}}}{p_{\mathrm{bulk}}}\right)^{0.25}\exp\left(-\frac{E_{\mathrm{act,ca}}}{RT}\right) \tag{20}$$

Here we have the pre-exponential factor γ which is defined by calibrating the simulated results against the experimental values. By expressing the activation overpotential with the following equation.

$$E-\eta_{\mathrm{act}} = \phi_{\mathrm{io}}-\phi_{\mathrm{el}} \tag{21}$$

and using the relations

$$\begin{aligned} i_{\mathrm{reac}} &= \frac{\mathrm{d}i_{\mathrm{el}}}{\mathrm{d}r}+\frac{1}{r}i_{\mathrm{el}} \\ &= -\frac{\mathrm{d}i_{\mathrm{io}}}{\mathrm{d}r}-\frac{1}{r}i_{\mathrm{io}} \end{aligned} \tag{22}$$

$$\begin{cases} \dfrac{\mathrm{d}\phi_{\mathrm{io}}}{\mathrm{d}r} = i_{\mathrm{io}}\rho_{\mathrm{io,eff}} \\ \dfrac{\mathrm{d}\phi_{\mathrm{el}}}{\mathrm{d}r} = i_{\mathrm{el}}\rho_{\mathrm{el,eff}} \end{cases} \tag{23}$$

we can derive following equation

$$\frac{\mathrm{d}^2\eta_{\mathrm{act}}}{\mathrm{d}r^2} = (\rho_{\mathrm{el}}+\rho_{\mathrm{io}})i_{\mathrm{reac}}+\frac{\mathrm{d}^2E}{\mathrm{d}r^2} \tag{24}$$

In deriving Eq. (24), Eq. (22) was simplified by ignoring the second terms of the right sides by applying narrow slit approximation. With the boundary conditions:

$$\begin{cases} r=r_{an} & i_{\mathrm{io}}=i & i_{\mathrm{el}}=0 \\ r=r_{\mathrm{el}} & i_{\mathrm{io}}=0 & i_{\mathrm{el}}=i \end{cases} \tag{25}$$

activation overpotential of the cell can be calculated.

Additionally, a steam reformation and gas shift reaction of methane is applied to the numerical model. Gas shift reaction is considered fast enough thus assumed being in equilibrium. On the other hand, the steam reforming reaction is dominated by its rate of reaction. For the present study, the reaction rate was chosen as Eq. (26), which is taken from the results of Noro et al.[8], who carried out a reforming experiment to determine it by applying the same anode material of the present experimental investigation.

(26)

5. RESULTS OF EXPERIMENTAL AND NUMERICAL STUDIES

Numerically and experimentally obtained voltage-current curves for dry and humidified hydrogen fuel are shown in Fig. 7-a. The numerical result shows a good agreement with the experimental result especially for dry hydrogen. However, numerical simulation tends to overestimate the cell performance when steam is introduced into the fuel. Since the deviation between numerical and experimental results increase with increase in steam content, it is considered that the activation overpotential is possibly underestimated. Eq. (19) shows that the activation overpotential decreases with increase in steam content. This tendency does appear in the numerical results, yet the real case is found to be more sensitive to the amount of steam. This suggests a possible further improvement of the prediction of a cell performance by the present numerical model.

Similar trends in the comparisons between experimental and numerical results can be seen in Fig. 7-b, in which results when humidified methane is introduced as the fuel. There is a good agreement between the experimental and numerical results at low S/C but the deviation increases as S/C increases which could be explained again by the underestimation of activation overpotential.

Fig. 7-b also shows that a significant drop in cell performance appears when methane with steam is fed as fuel rather than humidified hydrogen. To investigate the reason for this, additional numerical simulations are performed for methane with S/C = 1 excluding the endothermic effect, although it is unrealistic but effective to separate different issues. The result is also shown in Fig. 7-b. A minor drop in the cell performance of methane fuel without endothermic effect from dry hydrogen is considered mainly due to the decrease in Nernst potential. The cell performance drops even further when the endothermic phenomenon is included, which shows the importance of studying the temperature profile in

detail to understand the reason why the cell performance decreases when methane with steam is fed as fuel.

The temperature distribution of a cell applied with different fuel compositions is shown in Fig. 8. This non-uniform distribution in the axial direction causes various overpotential increase. One major increase is the ohmic resistance. Amount of current produced increases towards the fuel outlet region of the cell as shown also in Fig. 8, and as a result, a large current flows a long distance from the inlet region of the cell where the current collector is located. This causes a large voltage drop, and becomes the main cause of the decrease in cell performance when methane is applied.

6. CONCLUSION

A one-dimensional numerical simulation of a tubular SOFC is conducted applying the micro-structural parameters obtained from FIB-SEM images. Slight deviations were found between numerical simulation and experiment when the steam content of the fuel is increased. However, it can be concluded that the cell performance can be predicted to a good extent especially for low steam ratios. Through the numerical calculation, important guides are clearly shown in constructing an SOFC system. Cares must be taken especially at the fuel inlet region of the SOFC. The temperature drop due to methane reforming reaction is considered the main reason for the drop in cell performance. This knowledge helps to optimize the location of the catalyst bed for the fuel reformer, which is currently investigated by the present authors. It was also clarified that the electrochemical reaction is another crucial issue, which one should investigate further.

ACKNOWLEDGEMENTS

The authors would like to thank Prof. Kimijima with whom they had fruitful discussions in many regards.

REFERENCES

(1) Suzuki, M., Fukagata, K., Shikazono, N. and Kasagi, N., *Proc. Thermal Engineering Conference*, pp. 263-264 (2005)

(2) Sekiguchi, T. and Shikazono, N., *Proc. Mechanical Engineering Congress, 2007 Japan*, pp. 43-44 (2007)

(3) Shikazono, N., Sakamoto, Y., Yamaguchi, Y. and Kasagi, N., *J. Power Sources*, Vol. 193, pp. 530-540 (2009).

(4) Iwai, H. et al., *J. Power Sources*, 195 (4) pp. 955-961 (2010).

(5) Suwanwarangkul, R., Croiset, E., Fowler, M. W., Douglas, P. L. , Entchev, E. and Douglas, M. A. *J. Power Sources*, Vol. 122, pp. 9-18 (2009).

(6) de Boer, B., Ph. D. thesis, Univ. of Twente, The Netherland (1998)

(7) Costamagna, P. et al., *Electrochimica Acta*, Vol.43 Nos 3-4 (1998), 375-394.

(8) Noro, Y., Ichikawa, T. and Kimijima, S., *Proc. 14th National Symposium on Power and Energy Systems*, pp. 193-194 (2009).

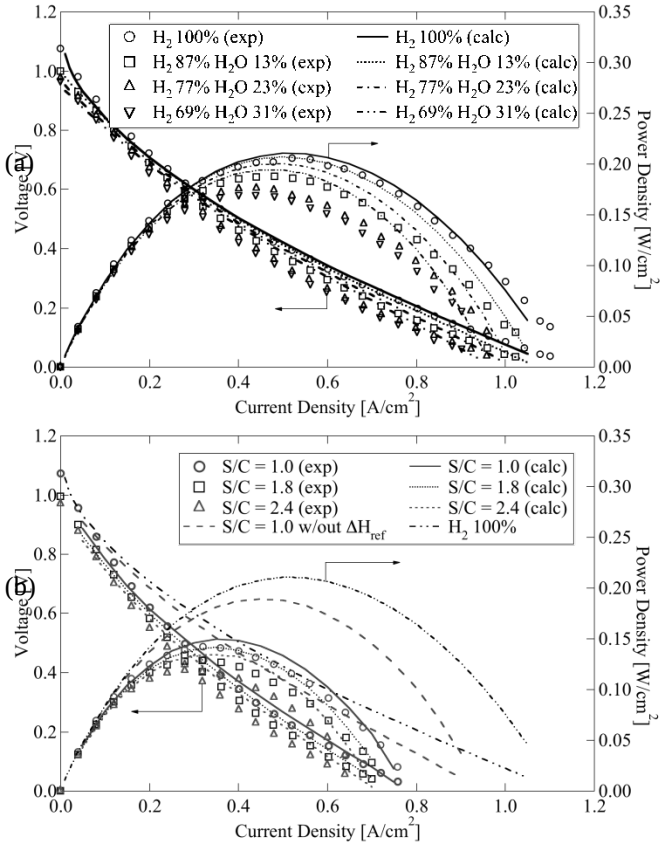

Fig. 7. Comparison of Experiment and Simulation (a) humidified hydrogen and (b) humidified

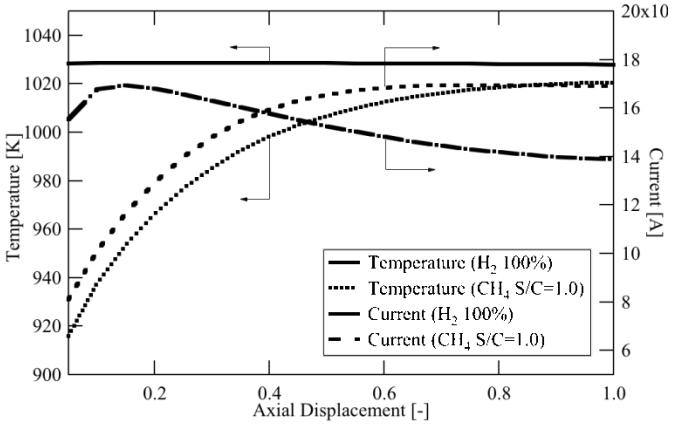

Fig 8. Temperature and current distribution